Supplementary Materials

Iron-doped poly(amidoamine)-based carbon dots with multienzyme-mimetic activities for dual-mode fluorescence and colorimetric detection of dichlorvos and Cr(VI)

Xinyi Feng [a], Yuqing Fu [a], Zhanqiu Tang [a], Hongyuan Tian [a], Zhenglong Wu [b], Weidong Qin [a,*]

[a] College of Chemistry, Beijing Normal University, Beijing 100875, China
[b] Analytical and Testing Center, Beijing Normal University, Beijing 100875, China

*Corresponding author:
Weidong Qin
E-mail: qinwd@bnu.edu.cn
Phone Number: 86-10-58802531

S1. Effect of the precursor molar ratio

The composition of the precursors plays a crucial role in determining the enzyme-mimicking properties of the carbon dots. Consequently, the molar ratio of G0-PAMAM: potassium ferricyanide: urea was systematically examined to optimize the multi-enzymatic performance of PAMAM-Fe CDs. As listed in Table S1, PAMAM-Fe CDs synthesized from eight precursor compositions (designed CDs-1 ~ CDs-8) were studied. Fig. S1 depicts the UV-vis spectra for characterizing the POD, OXD, CAT and SOD-mimetic activities of the CDs using the methods described in Section 2.4 of the manuscript. To facilitate evaluation, the enzymatic activities of the CDs were categorized as strong, medium, weak, or undetectable (N.D.) based on their absorbance values, according to the criteria outlined below.

POD: N.D., $A_{652\ nm}$ (0-0.030); weak, $A_{652\ nm}$ (0.031-0.120); medium, $A_{652\ nm}$ (0.121-0.600); strong, $A_{652\ nm}$ (>0.600);

OXD: N.D., $A_{652\ nm}$ (0-0.010); weak, $A_{652\ nm}$ (0.011-0.050); medium, $A_{652\ nm}$ (0.051-0.200); strong, $A_{652\ nm}$ (>0.200);

CAT: N.D., $A_{452\ nm}$ (0.460-0.466); weak, $A_{452\ nm}$ (0.440-0.459); medium, $A_{452\ nm}$ (0.200-0.439); strong, $A_{452\ nm}$ (<0.200);

SOD: N.D., $A_{560\ nm}$ (1.200-1.221); weak, $A_{560\ nm}$ (1.100-1.199); medium, $A_{560\ nm}$ (0.800-1.099); strong, $A_{560\ nm}$ (<0.800).

Our results indicate that the optimal multi-enzymatic performance of PAMAM-Fe CDs was achieved using precursors G0-PAMAM, potassium ferricyanide, and urea at a molar ratio of 1:1:0.5.

Table S1 Influence of precursor composition on the multi-enzymatic performance

Enzyme-like activity	The molar ratio of G0-PAMAM: Potassium ferricyanide: Urea							
	1:1:0	1:0:1	0:1:1	1:1:1	1:1:0.7	1:1:0.5	1:1:0.3	1:0.5:0.25
	CDs-1	CDs-2	CDs-3	CDs-4	CDs-5	CDs-6	CDs-7	CDs-8
POD	medium	weak	weak	weak	medium	strong	medium	weak
OXD	weak	weak	weak	weak	medium	strong	weak	N.D.[a]
CAT	medium	weak	N.D.	weak	medium	strong	medium	N.D.
SOD	medium	medium	medium	weak	medium	strong	medium	weak

[a] undetectable

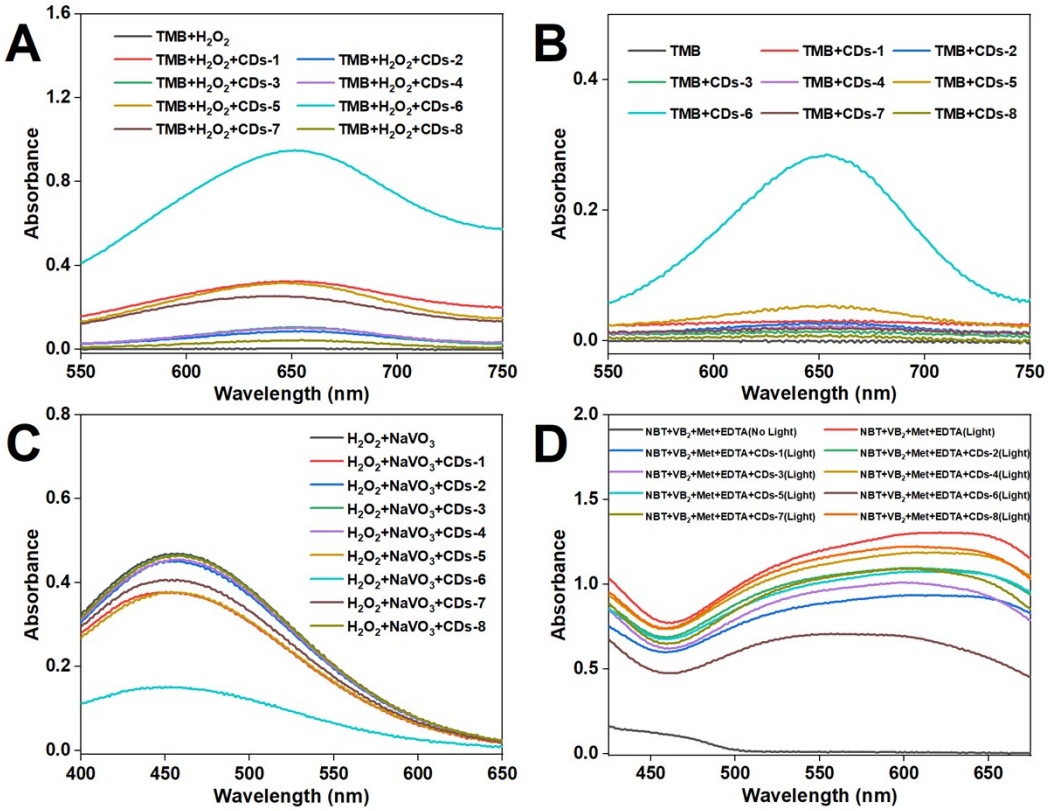

Fig. S1 Influence of precursor composition on multi-enzymatic performance. (A) UV–vis absorption spectra of the peroxidase-like colorimetric system after 15 minutes of reaction; (B) UV–vis absorption spectra of the oxidase colorimetric system after 15 minutes of reaction; (C) UV–vis absorption spectra of the catalase-like evaluation system after 30 minutes of reaction; (D) Visible absorption spectra of the superoxide dismutase-like evaluation system following a 10-minute incubation under 365 nm light irradiation at an intensity of 12.80 mW/cm². The molar ratios of the precursors for CD-1 through CD-8 are listed in Table S1.

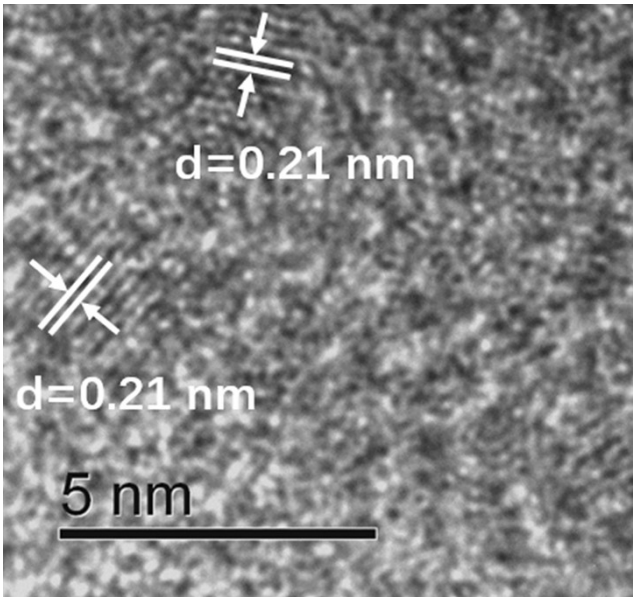

Fig. S2 High-resolution TEM image of the PAMAM-Fe CDs

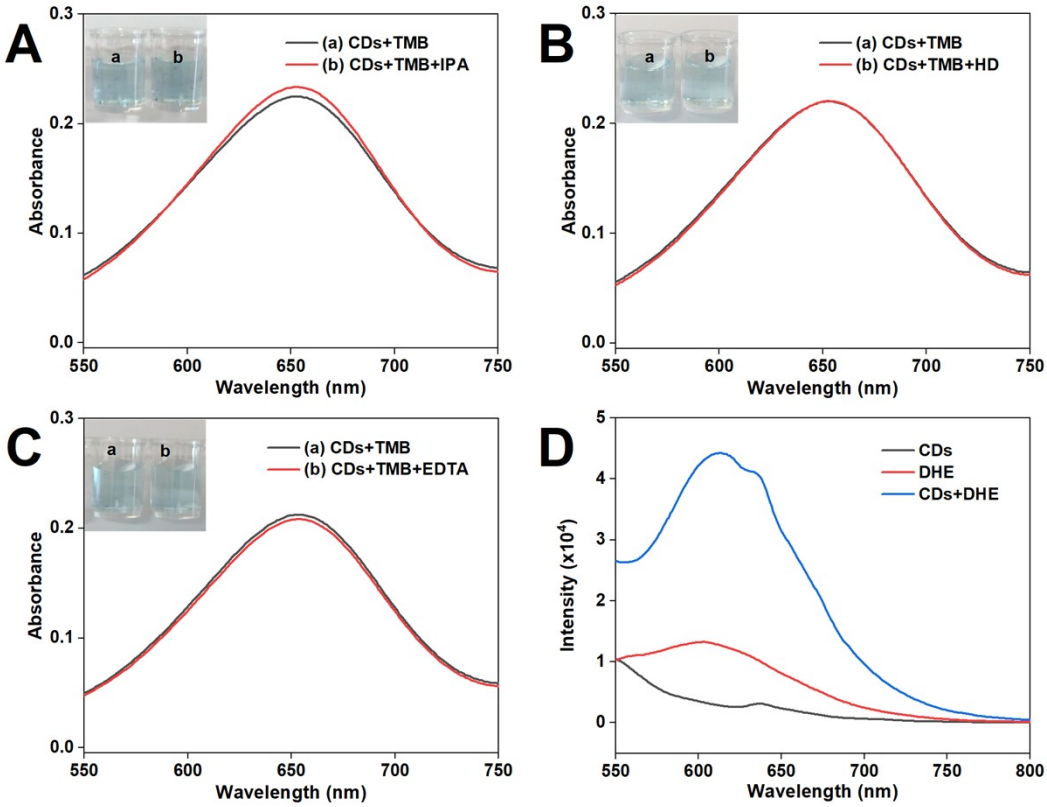

Fig. S3 (A) ·OH verification test in the (a) absence or (b) presence of IPA; (B) $^1O_2$ validation analysis in the (a) absence or (b) presence of HD; (C) h^+ verification test in the (a) absence or (b) presence of EDTA; and (D)fluorescence spectra of the PAMAM-Fe CDs, DHE, and PAMAM-Fe CDs + DHE after a reaction time of 30 min.

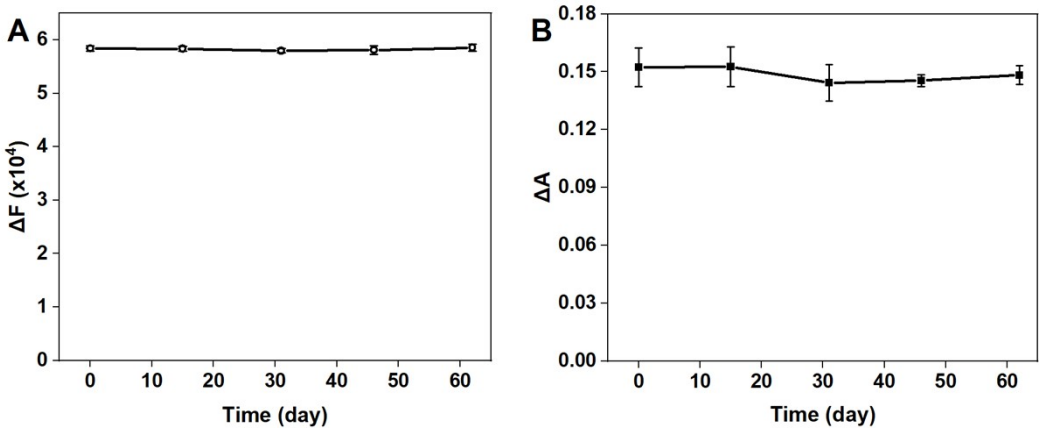

Fig. S4 Stability of PAMAM-Fe CDs stored for different durations (0, 15, 31, 46, and 62 days). (A) Response of dichlorvos at a concentration of 0.01 μg/mL using a detection system comprising PAMAM-Fe CDs, H_2O_2, Rh6G, and KI; (B) Response of Cr(VI) at a concentration of 2.5 μM using a detection system comprising PAMAM-Fe CDs and TMB.

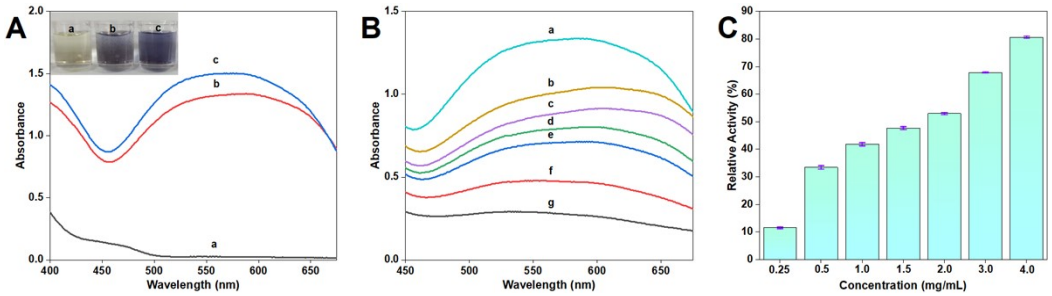

Fig. S5 (A) Visible absorption spectra of a mixture solution of NBT, riboflavin, methionine and EDTA under various conditions. (a) Blank control without light irradiation, (b) in the absence of nanomaterials with light irradiation, and (c) in the presence of PAMAM-Fe CDs with light irradiation; (B) scavenging efficiency of superoxide radicals with various concentrations of the PAMAM-Fe CDs toward superoxide radicals. (a) 0 mg/mL, (b) 0.5 mg/mL, (c) 1.0 mg/mL, (d) 1.5 mg/mL, (e) 2.0 mg/mL, (f) 3.0 mg/mL, and (g) 4.0 mg/mL; and (C) the relative SOD-like activity of the PAMAM-Fe CDs.

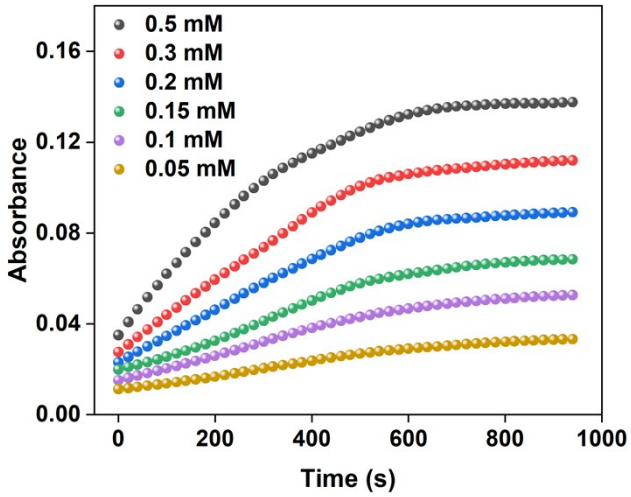

Fig. S6 Time-dependent absorbance changes at 652 nm for the PAMAM-Fe CDs + TMB system at various TMB concentrations (0.05, 0.10, 0.15, 0.20, 0.30, and 0.50 mM).

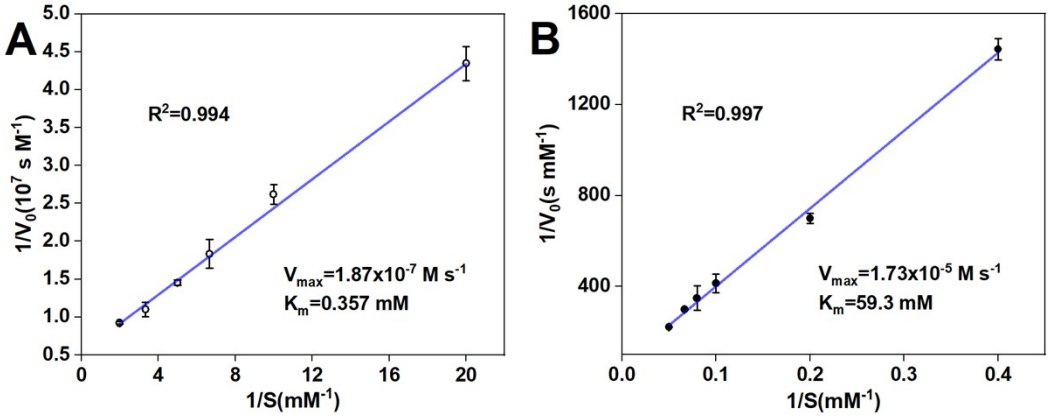

Fig. S7 Enzyme kinetics of the (A) oxidase-like activity and (B) catalase-like activity of the PAMAM-Fe CDs.

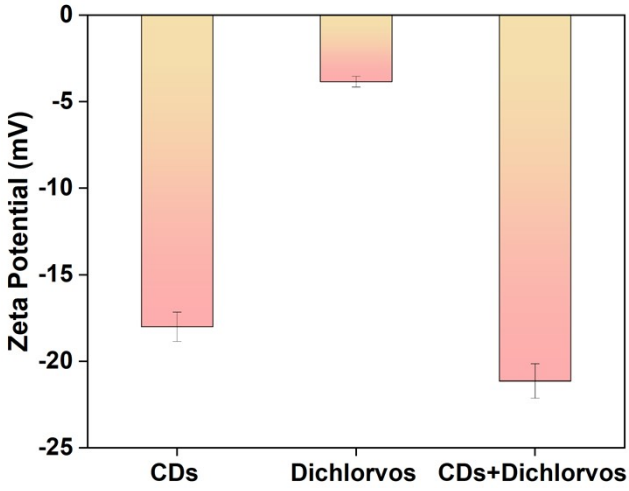

Fig. S8 Zeta potentials of the CDs, dichlorvos, and the CDs + dichlorvos at pH 9.8.

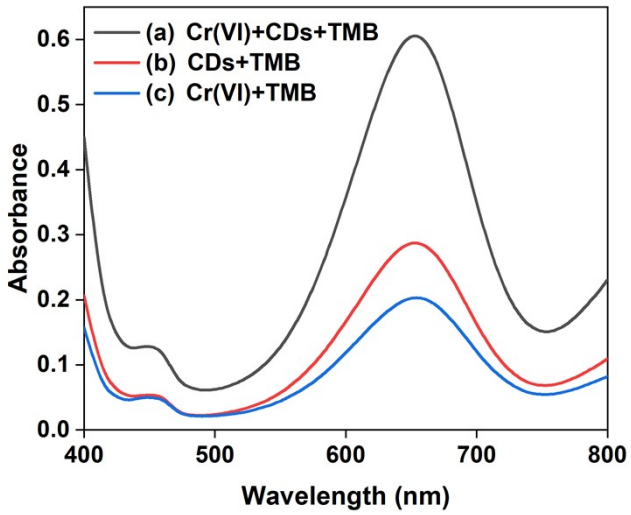

Fig. S9 UV–vis absorption spectra of several systems. (a) Cr(VI) + CDs +TMB, (b) CDs +TMB, and (c)Cr(VI) +TMB. The peak height at 652 nm ($\Delta A_{652\ nm}$) of curve a exceeded the combined peak height of curve b and curve c, which suggested that Cr(VI) had a synergistic effect on the CD-catalyzed oxidation of TMB.

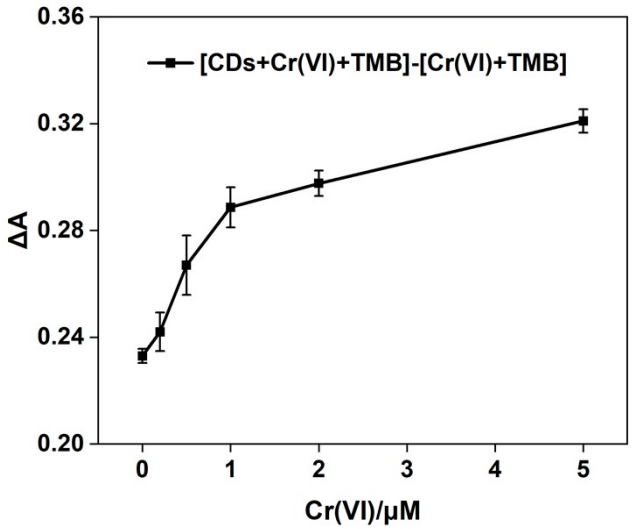

Fig. S10 Difference in peak absorbance (ΔA) between the Cr(VI)+CDs +TMB system and the Cr(VI)+TMB system at 652 nm as a function of the Cr(VI) concentration. ΔA increases with increasing Cr (VI) concentration, which indicated that Cr (VI) enhances the oxidase-like activity of CDs and synergistically oxidizes TMB.

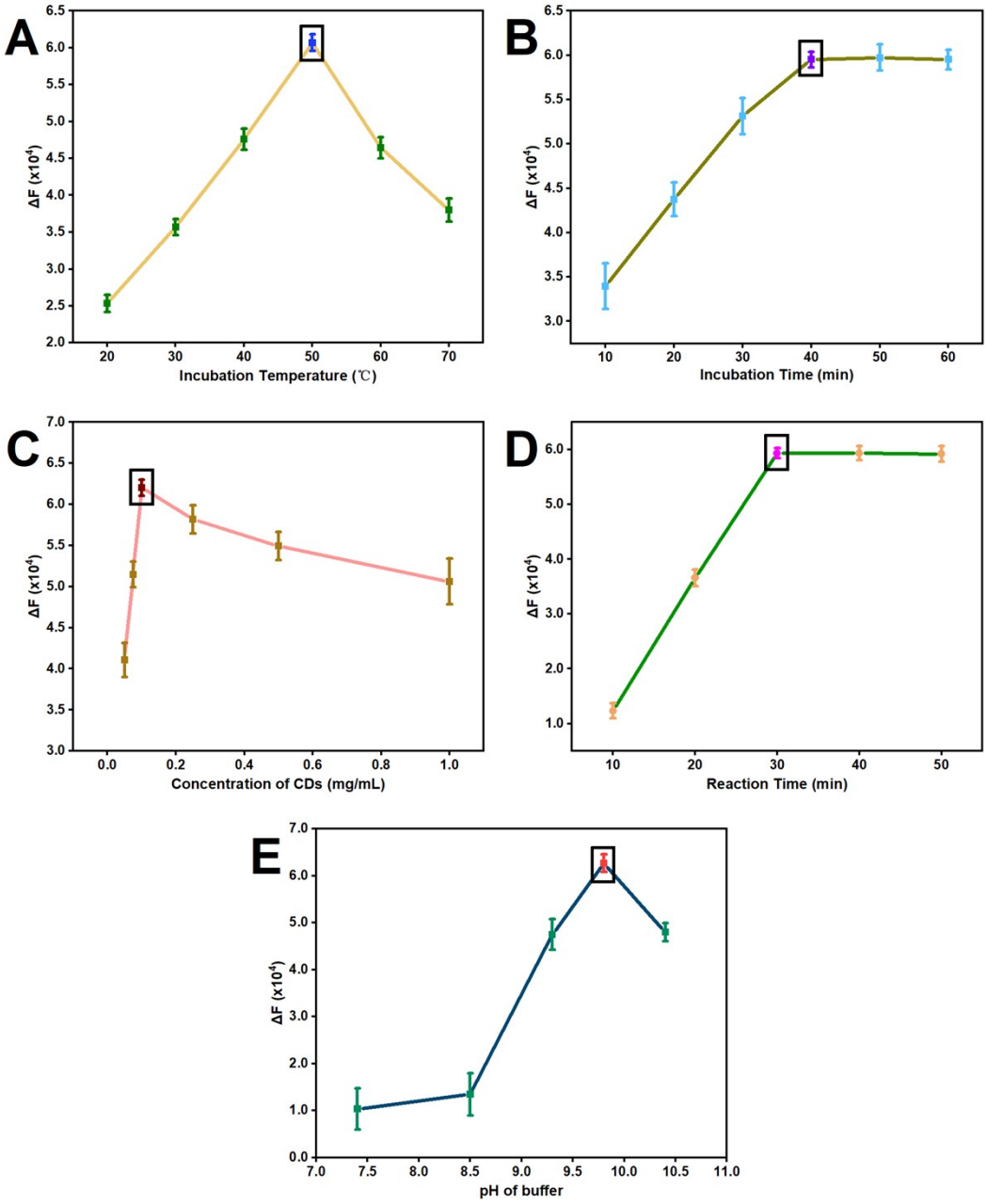

Fig. S11 Optimization of the experimental conditions for dichlorvos detection. (A) Incubation temperature, (B) incubation time, (C) concentration of the PAMAM-Fe CDs, (D) reaction time, and (E) pH of the buffer.

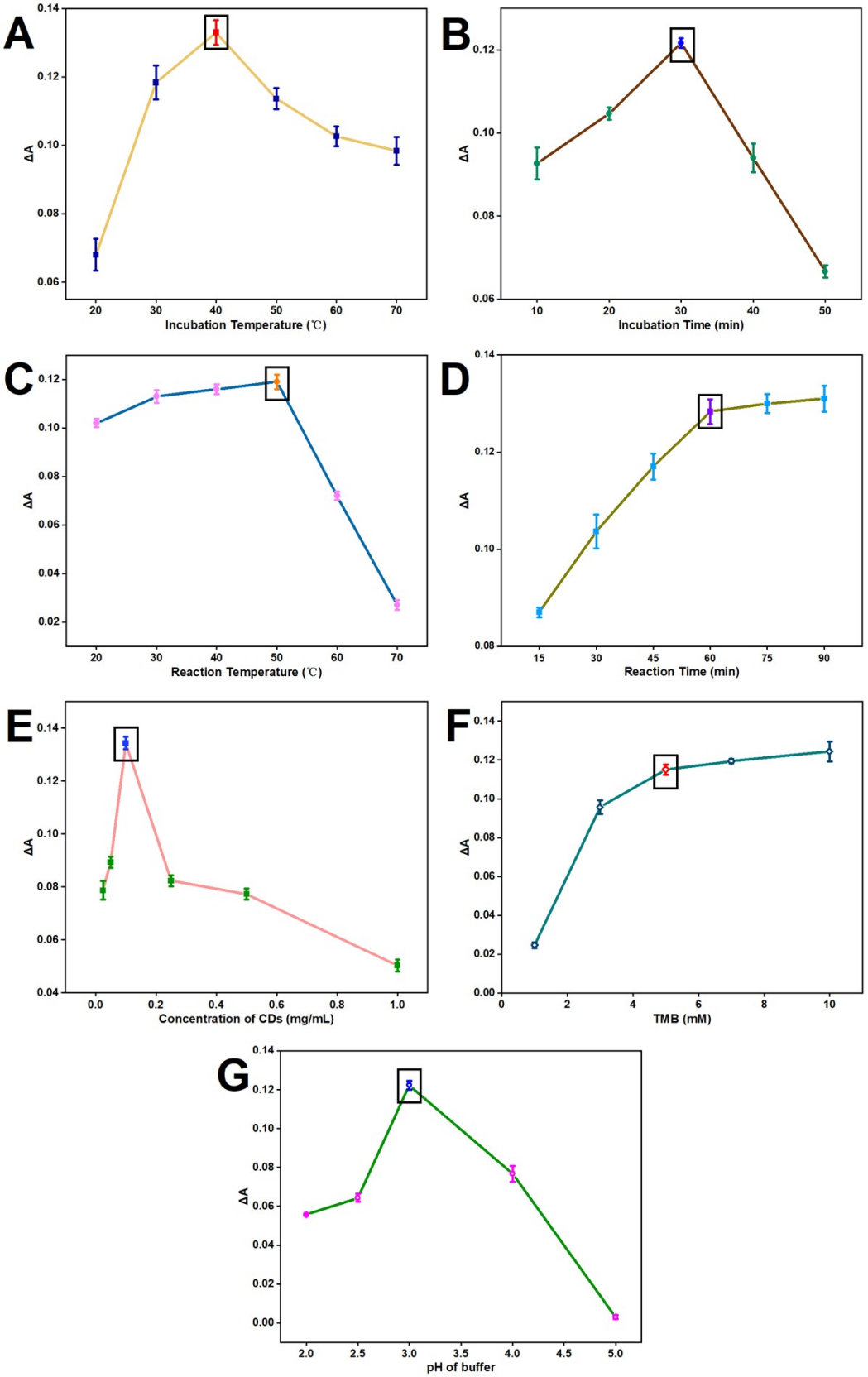

Fig. S12 Optimization of experimental conditions for Cr(VI) detection. (A) Incubation temperature, (B) incubation time, (C) reaction temperature, (D) reaction time, (E) concentration of the PAMAM-Fe CDs, (F) concentration of TMB, and (G) pH of the buffer.

Table S2 Comparison of kinetic parameters of the PAMAM-CDs and other reported oxidase-like materials

Catalyst	Substrate	Km (mM)	Vm (10^{-8} M s^{-1})	Reference
PAMAM-Fe CDs	TMB	0.357	18.7	This work
CeO_2	TMB	0.420	10.04	[1]
PAA-CeO_2	TMB	0.597	3.05	[2]
Fe-N-C	TMB	1.81	0.06	[3]
CoN_5SA/CNF	TMB	0.682	0.177	[4]
H_2O_2-nanoceria	TMB	0.76	4.50	[5]
CuO NPs-POM	TMB	0.90	3.72	[6]
Cu_3/ND@G	TMB	2.89	11.5	[7]
Co-SAs@NC	TMB	3.48	0.459	[8]
Fe-NDs	TMB	0.55	4.01	[9]
CDs/AgNPs	TMB	0.60	0.12	[10]
Cu-CeO_2 NPs	TMB	0.71	5.56	[11]

Table S3 Comparison of kinetic parameters of the PAMAM-CDs with other reported catalase-like materials

Catalyst	Substrate	Km (mM)	Vm (10^{-6} M s^{-1})	Reference
PAMAM-Fe CDs	H_2O_2	59.3	17.3	This work
AgPt NPs	H_2O_2	62.98	6.10	[12]
Co_3O_4 nanocubes	H_2O_2	63.90	1.23	[13]
Ti_3C_2Tx	H_2O_2	85.58	0.01	[14]
Co,N-CNC	H_2O_2	65.08	9.86	[15]
N-PCNSs-3	H_2O_2	66.25	0.268	[16]
N-PCNSs-5	H_2O_2	154	0.246	[16]
Pd cubes	H_2O_2	102.4	2.2	[17]
Pd octahedrons	H_2O_2	135.1	5.9	[17]
Fe^{3+}/AMP CPs	H_2O_2	112.2	2.4	[18]

Table S4 Comparison of different assays for the detection of dichlorvos

Material/Platform	Detection method	LOD (μg/mL)	Linear Range (μg/mL)	Reference
PAMAM-Fe CDs	Fluorometry	0.0000169	0.0001-10	This work
DTAB-ZnTPyP	Colorimetry	0.00102	0.005-0.045	[19]
Cu-CDs	Colorimetry	0.0017	0.004-0.07	[20]
FeMnOx	Colorimetry	0.000267	0.001-3	[21]
AuNRs@MS@TiO_2-CS/GC	Electrochemistry	0.0012	0.004-3	[22]
AChE@PILs@Au NPs/GCE	Electrochemistry	0.000039	0.00013-1.4	[23]
nanogold/mercaptomethamidophos	Electrochemistry	0.000022	0.0001-1.5	[24]
CD-CdTe QD	Fluorometry	0.00038	0.001-0.04	[25]
MnO_2 NSs-CQDs/AR	Fluorometry	0.0012	0.004-0.120	[26]
SiQDs/CuNCs	Fluorometry	0.00134	0.005-2	[27]
CDs-Fe	Photothermal	0.00485	0.005-0.65	[28]

Table S5 Comparison of different assays for the detection of Cr(VI)

Material/Platform	Detection method	LOD (μM)	Reference
PAMAM-Fe CDs	Colorimetry	0.0418	This work
IMBO NCs	Colorimetry	0.50	[29]
H-Fe-POP	Colorimetry	0.23	[30]
FP CoS	Colorimetry	0.0756	[31]
PANI/GQDs	Electrochemistry	1.87	[32]
PZrS nanocomposite	Electrochemistry	0.0643	[33]
TA-CDs	Fluorometry	0.57	[34]
CS-CDs	Fluorometry	0.59	[35]
CPCTA-3	Fluorometry	1.12	[36]
PcOP-Fe	Photochemistry	0.18	[37]

S2. Detect of dichlorvos and Cr(VI) in soil samples

Soil treatment: Soil samples were collected from the vegetable garden within the Green Garden at BNU and processed according to established protocols[38] with minor modifications. Briefly, after removing stones and plant roots, the samples were crushed and dried at 60 °C until a constant weight was achieved. Subsequently, the dried soil was finely ground using a mortar and passed through a 100-mesh sieve. A 1 g aliquot of the sieved soil was transferred into a centrifuge tube, to which 1 mL of Cr(VI) or dichlorvos solutions at varying concentrations was added, resulting in Cr(VI) concentrations of 0.5, 1, and 2 μM, and dichlorvos concentrations of 0.0005, 0.1, 0.15, 0.25, and 0.5 μg/g. The samples were then extracted at room temperature for 2 hours, followed by centrifugation at 16,000 rpm for 10 minutes. The supernatant was collected, filtered through a 0.22 μm membrane filter, and adjusted to a final volume of 1 mL with triple-distilled water.

Table S6 Detection of dichlorvos in soil samples (n=3)

Sample	Added (μg/mL)	Found (μg/mL)	Recovery (%)	RSD (%)
Soil	0	-	-	-
	0.0005	0.000487	97.4	2.90
	0.1	0.102	102	0.876
	0.15	0.150	100	2.61

Table S7 Detection of Cr(VI) in soil samples (n=3)

Sample	Added (μM)	Found (μM)	Recovery (%)	RSD (%)
Soil	0	-	-	-
	0.5	0.484	96.8	1.60
	1	1.03	103	4.38
	2	2.01	100	1.47

S3. Comparison with commercial detection kits

S3.1 Commercial dichlorvos detection kits

Rapid detection of dichlorvos was conducted using a commercially available colloidal gold test kit (Yuxiang Biotechnology, Jiangsu, China), which includes a control line (C line) and a test line (T line). The detection limit of the kit was established at 0.2 mg/kg, equivalent to 0.2 μg/mL under the conditions of this study. Samples with dichlorvos concentrations exceeding this threshold were classified as positive, while those below it were considered negative. During analysis, if the color intensity of T line was equal to or greater than that of the C line, the result was interpreted as negative, indicating either the absence of the analyte or its presence at concentrations below the detection limit. Conversely, if the color intensity of T line was weaker than that of the C line or if the T line failed to develop color, the result was deemed positive, signifying that the analyte concentration in the sample met or exceeded the detection limit.

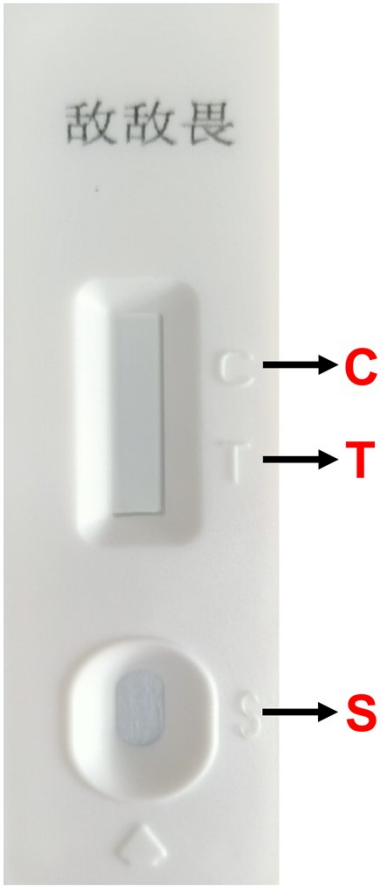

Fig. S13 Schematic diagram of dichlorvos detection strip

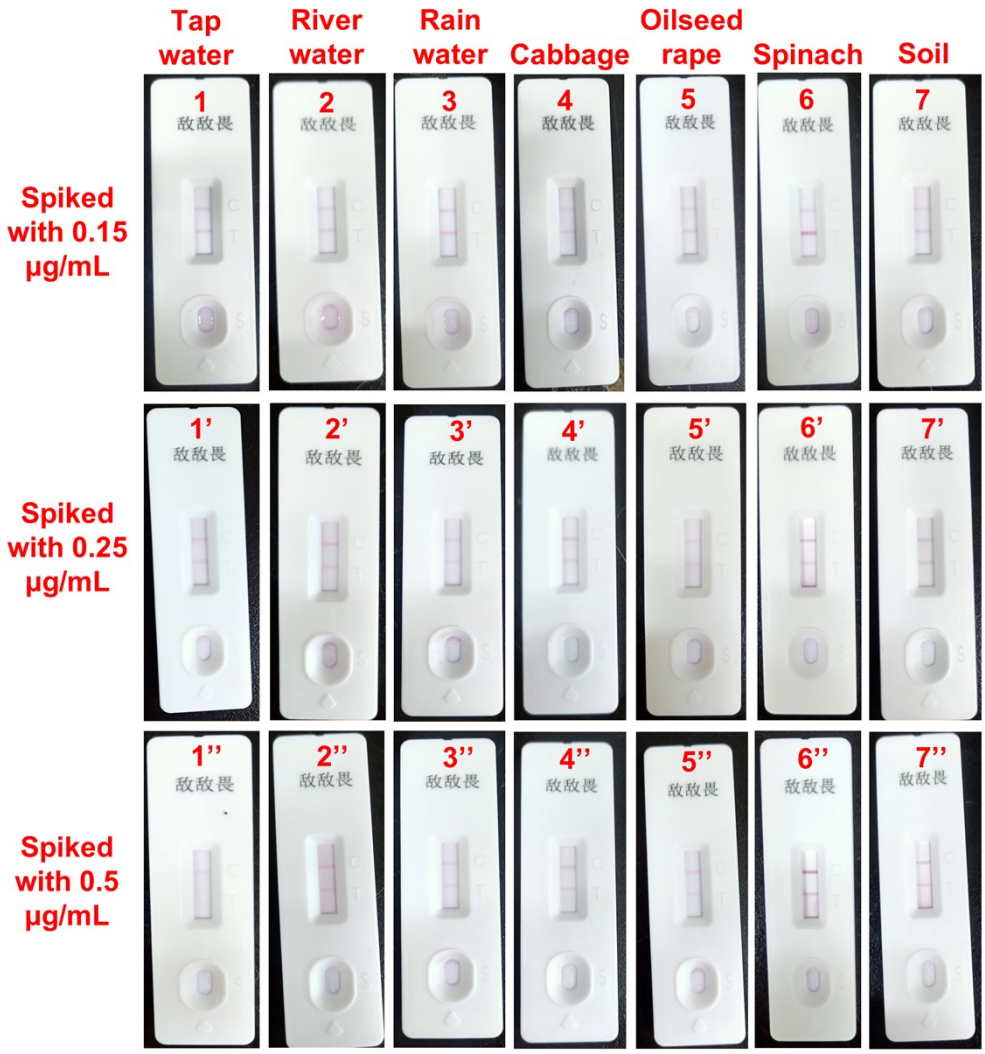

Fig. S14 Rapid detection of dichlorvos using commercial colloidal gold kits. 1-7 showed negative results for tap water, river water, rain water, cabbage, spinach, rapeseed, and soil samples with a spiked concentration of 0.15 μg/mL of dichlorvos; 1'-7' showed positive results for these samples with a spiked concentration of 0.25 μg/mL of dichlorvos; 1''-7'' showed positive results for these samples with a spiked concentration of 0.5 μg/mL of dichlorvos.

S3.2 Commercial Cr(VI) detection kits

Detection of Cr(VI) was performed using a commercially available water quality test kit (Luheng Environmental Technology, Zhejiang, China). The kit's detection range was 0.01–1.0 mg/L, with calibration points at concentrations of 0.01, 0.025, 0.05, 0.10, 0.25, 0.50, 0.75, and 1.00 mg/L, corresponding to 0.192, 0.481, 0.962, 1.92, 4.81, 9.61, 14.4, and 19.2 μM, respectively.

Fig. S15 Schematic diagram of Cr(VI) detection card

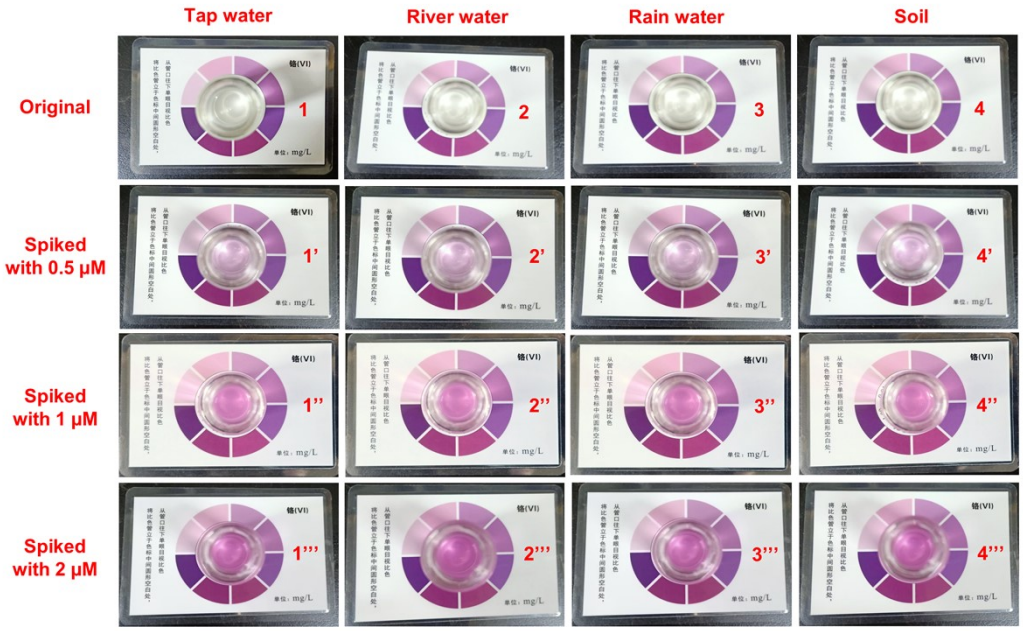

Fig. S16 Detection of Cr(VI) utilizing commercially available water quality test kits. Panels 1 through 4 present the results for tap water, river water, rain water, and soil samples, respectively. Panels 1' to 4' display the outcomes for the same samples spiked with 0.5 μM of Cr(VI). Panels 1'' to 4'' correspond to the samples with a spiked concentration of 1 μM Cr(VI), while panels 1''' to 4''' show the results for samples spiked with 2 μM Cr(VI).

Table S8 Detection of dichlorvos in real samples (n=3) and comparison with commercial detection kits

Sample	Added (μg/mL)	Found (μg/mL)	Recovery (%)	RSD (%)	Commercial detection kits	Entry in Fig. S14
Tap water	0.15	0.159	106	0.716	Negative	1
	0.25	0.259	104	1.42	Positive	1’
	0.5	0.497	99.4	1.56	Positive	1’’
River water	0.15	0.146	97.3	2.63	Negative	2
	0.25	0.257	103	0.752	Positive	2’
	0.5	0.497	99.4	0.907	Positive	2’’
Rain water	0.15	0.153	102	1.00	Negative	3
	0.25	0.256	102	1.26	Positive	3’
	0.5	0.524	105	1.77	Positive	3’’
Cabbage	0.15	0.151	101	1.20	Negative	4
	0.25	0.245	98.0	3.48	Positive	4’
	0.5	0.474	94.8	2.89	Positive	4’’
Oilseed rape	0.15	0.159	106	3.04	Negative	5
	0.25	0.238	95.2	1.45	Positive	5’
	0.5	0.473	94.6	1.52	Positive	5’’
Spinach	0.15	0.150	100	4.03	Negative	6
	0.25	0.239	95.6	2.31	Positive	6’
	0.5	0.507	101	3.60	Positive	6’’
Soil	0.15	0.150	100	2.61	Negative	7
	0.25	0.251	100	1.77	Positive	7’
	0.5	0.524	105	2.19	Positive	7’’

Table S9 Detection of Cr(VI) in real samples (n=3) and Comparison with commercial detection kits

Sample	Added (μM)	Found (μM)	Recovery (%)	RSD (%)	Commercial detection kits (μM)	Entry in Fig. S16
Tap water	0	-	-	-	-	1
	0.5	0.432	86.4	2.36	0.481	1’
	1	0.992	99.2	1.81	0.962	1’’
	2	1.97	98.5	1.69	1.92	1’’’
River water	0	0.156	-	2.27	-	2
	0.5	0.587	86.2	4.06	0.481	2’
	1	1.12	96.4	2.24	0.962	2’’
	2	2.28	106	4.51	1.92	2’’’
Rain water	0	-	-	-	-	3
	0.5	0.456	91.2	3.52	0.481	3’
	1	1.08	108	2.29	0.962	3’’
	2	1.96	98.0	0.640	1.92	3’’’
Soil	0	-	-	-	-	4
	0.5	0.484	96.8	1.60	0.481	4’
	1	1.03	103	4.38	0.962	4’’
	2	2.01	100	1.47	1.92	4’’’

Reference

1. H. J. Cheng, S. C. Lin, F. Muhammad, Y. W. Lin and H. Wei, ACS Sens., 2016, 1, 1336-1343.
2. S. X. Zhang, S. F. Xue, J. J. Deng, M. Zhang, G. Y. Shi and T. S. Zhou, Biosens. Bioelectron., 2016, 85, 457-463.
3. Y. Wu, L. Jiao, X. Luo, W. Q. Xu, X. Q. Wei, H. J. Wang, H. Y. Yan, W. L. Gu, B. Z. Xu, D. Du, Y. H. Lin and C. Z. Zhu, Small, 2019, 15, 7, 1903108.
4. L. Huang, J. X. Chen, L. F. Gan, J. Wang and S. J. Dong, Sci. Adv., 2019, 5, 9, eaav5490.
5. J. Y. Zhang, J. Wang, J. Liao, Y. Lin, C. B. Zheng and J. W. Liu, ACS Appl. Mater. Interfaces, 2021, 13, 50236-50245.
6. Y. X. Xu, P. P. Li, X. J. Hu, H. Y. Chen, Y. Tang, Y. Zhu, X. H. Zhu, Y. Y. Zhang, M. L. Liu and S. Z. Yao, ACS Appl. Nano Mater., 2021, 4, 8302-8313.
7. F. C. Meng, M. Peng, Y. L. Chen, X. B. Cai, F. Huang, L. N. Yang, X. Liu, T. Li, X. D. Wen, N. Wang, D. Q. Xiao, H. Jiang, L. X. Xia, H. Y. Liu and D. Ma, Appl. Catal. B-Environ. Energy, 2022, 301, 7, 120826.
8. S. F. Cai, J. M. Liu, J. W. Ding, Z. Fu, H. L. Li, Y. L. Xiong, Z. Lian, R. Yang and C. Y. Chen, Angew. Chem.-Int. Edit., 2022, 61, 9, e202204502.
9. Y. Liu, J. H. Yan, Y. Huang, Z. H. Sun, H. J. Zhang, L. H. Y. Fu, X. W. Li and Y. R. Jin, Front. Bioeng. Biotechnol., 2022, 9, 11, 790849.
10. J. R. Zhu, Q. Q. Han, Q. L. Li, F. Wang, M. D. Dong, N. Y. Liu, X. Li, D. Chen, D. Z. Yang, Y. Z. Song and Y. L. Yang, Biomater. Sci., 2023, 11, 2711-2725.
11. J. Liu, Y. Zhu, Y. Fan, L. Gong, X. H. Zhu, Y. Y. Zhang, M. L. Liu and S. Z. Yao, J. Colloid Interface Sci., 2024, 654, 1054-1062.
12. M. Gharib, A. Kornowski, H. Noei, W. J. Parak and I. Chakraborty, ACS Mater. Lett., 2019, 1, 310-319.
13. J. S. Mu, L. Zhang, M. Zhao and Y. Wang, ACS Appl. Mater. Interfaces, 2014, 6, 7090-7098.
14. Q. Q. Qiao, J. Y. Wang, K. Long, L. W. Li, J. H. Chen, Y. H. Guo, Z. Q. Xu, Y. Kuang, T. J. Ji and C. Li, Nano Today, 2024, 54, 16, 102059.
15. T. T. Zhang, N. N. Lu, C. Wang, R. S. Zhang, W. J. Chen, Z. Q. Zhang and D. M. Xing, Chem. Eng. J., 2022, 437, 8, 135267.
16. K. L. Fan, J. Q. Xi, L. Fan, P. X. Wang, C. H. Zhu, Y. Tang, X. D. Xu, M. M. Liang, B. Jiang, X. Y. Yan and L. Z. Gao, Nat. Commun., 2018, 9, 11, 1440.
17. C. C. Ge, G. Fang, X. M. Shen, Y. Chong, W. G. Wamer, X. F. Gao, Z. F. Chai, C. Y. Chen and J. J. Yin, ACS Nano, 2016, 10, 10436-10445.
18. M. Z. Jiao, Z. J. Li, X. L. Li, Z. J. Zhang, Q. P. Yuan, F. Vriesekoop, H. Liang and J. W. Liu, Chem. Eng. J., 2020, 388, 9, 124249.
19. G. Q. Deng, H. Y. Chen, Q. Shi, L. X. Ren, K. Liang, W. J. Long, W. Lan, X. L. Han, Y. B. She and H. Y. Fu, Microchim. Acta, 2022, 189, 11, 375.
20. G. T. Yi, Z. W. Tao, W. F. Fan, H. Zhou, Q. F. Zhuang and Y. Wang, ACS Sustain. Chem. Eng., 2024, 12, 1378-1387.
21. S. G. Liu, H. Y. Wang, Q. Zhao, W. L. Gao, X. B. Shi and Z. H. Liu, Anal. Chim. Acta, 2024, 1292, 10, 342243.
22. H. F. Cui, T. T. Zhang, Q. Y. Lv, X. J. Song, X. J. Zhai and G. G. Wang, Biosens. Bioelectron., 2019, 141, 8, 111452.

23. Y. Wan, H. T. Wang, L. Zhang, Y. X. Chen, S. Li, J. Zhou, Q. Zhang and L. X. Xia, Microchim. Acta, 2022, 189, 12, 300.
24. G. Z. Zhao, B. H. Zhou, X. W. Wang, J. Shen and B. Zhao, Food Chem., 2021, 354, 7, 129511.
25. S. Huang, J. D. Yao, B. Li, G. Ning and Q. Xiao, Microchim. Acta, 2021, 188, 10, 318.
26. H. Mei, X. L. Zhu, Z. Q. Li, J. H. Jiang, H. L. Wang, X. D. Wang and P. P. Zhou, Food Chem., 2024, 434, 137507.
27. B. Y. Su, W. W. Wang, X. Y. Yang, D. Y. Chen and X. M. Chen, J. Food Compos. Anal., 2025, 143, 107603.
28. Y. Y. Yang, J. J. Xu, R. R. Zhou, Z. Y. Qin, C. H. Liao, S. Y. Shi, Y. X. Chen, Y. Guo and S. H. Zhang, Carbon, 2024, 219, 118831.
29. P. Li, Y. F. Li, M. Y. Qi and X. Zhang, Chem. Eng. J., 2024, 493, 11, 152686.
30. L. Q. Zhu, F. Yang, C. C. Lou, X. M. Zhang and Y. Z. Yang, Microchim. Acta, 2023, 190, 11, 339.
31. J. R. Guo, J. Wu, J. Z. Yang and J. H. He, Talanta, 2025, 285, 10, 127379.
32. E. Punrat, C. Maksuk, S. Chuanuwatanakul, W. Wonsawat and O. Chailapakul, Talanta, 2016, 150, 198-205.
33. M. H. Motaghedifard, S. M. Pourmortazavi and S. Mirsadeghi, Sens. Actuator B-Chem., 2021, 327, 9, 128882.
34. H. J. Chen, D. Li, Y. T. Zheng, K. Wang, X. B. Zhang, S. Zhou, S. S. Wei, F. Y. Yong, J. Nie, H. Y. Wen, J. Y. Wu, W. M. Xue and S. P. Huang, Sep. Purif. Technol., 2025, 356, 10, 129852.
35. Y. Q. Feng, R. X. Li, P. Zhou and C. Y. Duan, Microchem J., 2022, 180, 9, 107627.
36. J. Li, Y. K. Xi, H. Shao, Q. L. Ma, X. T. Dong and X. Li, Chem. Eng. J., 2025, 509, 12, 161359.
37. W. F. Ding, Z. Y. Mo, J. Qi, M. Y. Wang, J. Y. Zou, K. Wang, D. X. Gong, Y. J. Zhao, H. Miao and Z. Q. Zhao, Environ. Res., 2025, 264, 10, 120282.
38. X. C. Song, K. Z. Zhang, M. Lu, P. D. Bai and X. J. Huang, J. Chromatogr. A, 2025, 1760, 10, 466314.